JOURNAL OF THE ELECTROCHEMICAL SOCIETY

ELECTROCHEMICAL SCIENCE AND TECHNOLOGY

SOLID-STATE SCIENCE AND TECHNOLOGY

REVIEWS AND NEWS

VOL. 124, NO. 4

April 1977

JESOAN 124 (4) 475-636, 159C-176C

It makes the mapped leaky devices highly visible, it is free from the drawbacks associated with the anodic method, it is nondestructive, and it lends itself to repeated use on the same sample. It keeps the voltage drop across the devices constant, thus leading to reliable and interpretable results. It makes for clear distinction between leaky and nonleaky devices, probably because overpotential is reduced once a thin film of nickel has been plated; this effect is in direct contrast with the effect of the insulating anodic oxide film formed in the anodic method.

After mentioning all these virtues of the cathodic method, we must conclude by mentioning its limitation, which is essentially complementary to that of the anodic method. Specifically, it cannot be applied to n-p-n transistors that are completely isolated from the substrate. In modern integrated circuits, many transistors are so isolated. In such cases, the cathodic method would be useful in mapping, for example, leakage in the isolation itself. Another of the numerous possible applications would be the mapping of n-channel FET integrated circuits.

Acknowledgments

The author thanks Mr. Paul R. Poponiak for his skillful experimental assistance and Dr. T. H. Yeh for useful discussions.

Manuscript submitted Aug. 31, 1976; revised manuscript received Nov. 29, 1976. This was Paper 451 RNP presented at the Washington, D.C., Meeting of the Society, May 2-7, 1976.

Any discussion of this paper will appear in a Discussion Section to be published in the December 1977 JOURNAL. All discussions for the December 1977 Discussion Section should be submitted by Aug. 1, 1977.

Publication costs of this article were assisted by the IBM Corporation.

REFERENCES

1. G. H. Plantinga, *IEEE Trans. Electron Devices*, **ed-16**, 394 (1969).
2. M. V. Kulkarni, J. C. Hasson, and G. A. A. James, *ibid.*, **ed-19**, 1098 (1972).
3. D. K. Seto, F. Barson, and B. F. Duncan, in "Semiconductor Silicon 1973," H. R. Huff and R. R. Burgess, Editors, pp. 651-657, The Electrochemical Society Softbound Symposium Series, Princeton, N.J. (1973).
4. S. M. Hu, *J. Appl. Phys.*, **46**, 1465 (1975).
5. S. M. Hu, *ibid.*, **46**, 1470 (1975).
6. For example, see A. J. R. deKock, *Appl. Phys. Lett.*, **16**, 100 (1970). See also H. Shiraki, J. Matsue, and T. Kawamura, Proceedings of the Second Conference on Solid State Devices, Tokyo (1970).

Four-Point Sheet Resistance Measurements of Semiconductor Doping Uniformity

David S. Perloff, Frederick E. Wahl, and James Conragan

Signetics Corporation, Research and Development Laboratory, Sunnyvale, California 94086

ABSTRACT

A system is described for automatically measuring the sheet resistance of doped semiconductor wafers using either a conventional four-point probe or microelectronic van der Pauw resistors. Graphic display formats useful for conveying information about doping uniformity are discussed, and the tendency of random measurement error to degrade equivalue contour maps is illustrated. Excellent agreement is observed for sheet resistance data obtained from van der Pauw resistors which differ in area by more than three orders of magnitude. It is shown experimentally that the four-point probe and van der Pauw resistors may be used interchangeably for doping uniformity measurements.

The spatial uniformity of the processes employed in semiconductor microcircuit fabrication is an important determinant of the matching of components and of the yield of functional circuits. Even a highly controlled doping process such as ion implantation may be subject to intrinsic sources of variability which can adversely affect component matching (1, 2).

Parameters such as sheet resistance and film thickness have been shown to vary systematically over the surface of a processed silicon wafer (3, 4). The equivalue contour maps (topographs), which were used in Ref. (4) for exhibiting spatial variations, summarize a great deal of information in a compact and easily comprehended format. This method of display is, however, extremely sensitive to random measurement error, particularly when such error becomes comparable to the difference in parametric values at adjacent test sites.

In this paper, four-point sheet resistance measurement techniques are described which provide data sufficiently free of random error to justify the use of equivalue contour maps. It will be shown that the four-point probe (FPP) (5, 6) and van der Pauw resistors (7), although sampling areas of the wafer which differ by as much as five orders of magnitude, nevertheless provide comparable information about the spatial distribution of impurities.

Key words: four-point probe, resistor, silicon.

Data Acquisition System

A general-purpose system for the acqusition of four-point sheet resistance data is shown schematically in Fig. 1. This system consists of a standard X-Y probing apparatus, data terminal, recording devices, prober control, and sequencing and interface modules. Two of the four sample probes carry current supplied by a Keithley Model 225 constant (±0.005% stability) current supply; potential differences[1] are measured across the remaining two probes with a resolution of 10 μV by a Nonlinear Systems Corporation Model MX-1 digital voltmeter. The magnitude of the measurement current is adjusted to achieve a potential difference in the range of 30 ± 10 mV for both FPP and van der Pauw resistor measurements.

A rectangular array of up to 99 rows and 99 columns is employed for one-dimensional profiling as well as two-dimensional mapping of wafers. The wafer probe

[1] The polarity of the current supply is reversed and readings of the potential difference averaged to eliminate small offset voltages associated either with thermoelectric effects or instrumentation.

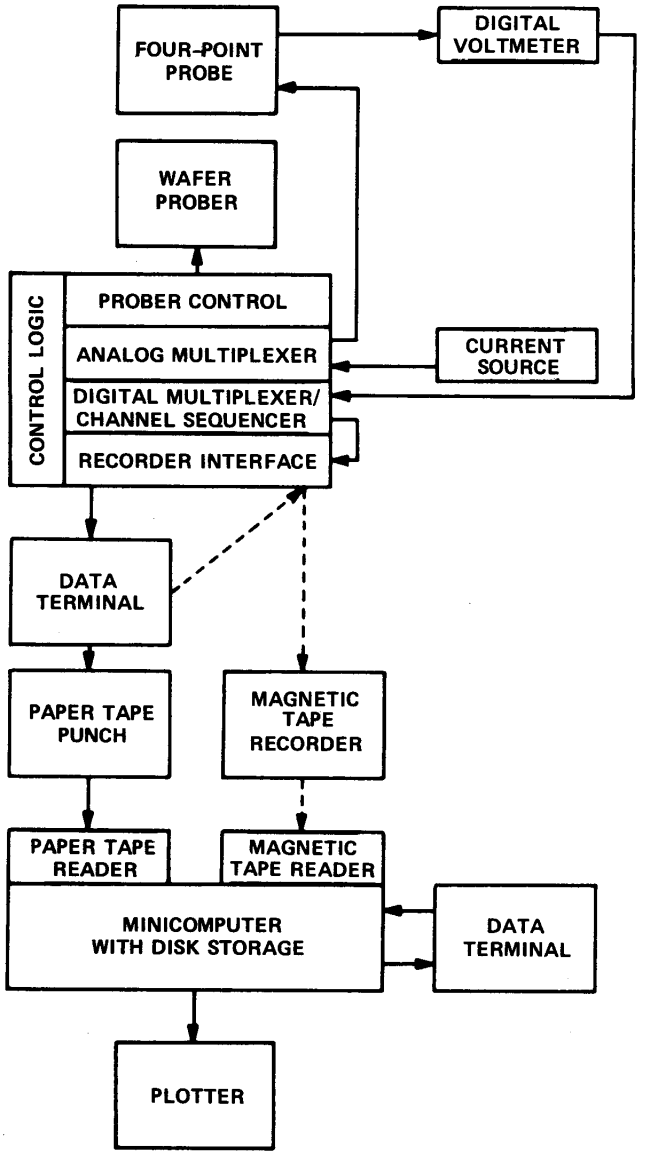

Fig. 1. Data acquisition system

step-and-repeat distances ΔX and ΔY may be varied between 10 and 999 mil in increments of 1 mil along both the X and Y axes of movement. At each test site, an analog multiplexer is used to switch analog signals. For each analog channel, a digital multiplexer and its associated digital channel sequencer select up to nine channels for transfer by the interface system to the recording device (paper tape punch or incremental magnetic tape recorder).

Data are analyzed off-line by a Digital Equipment Corporation Model PDP 11/40 minicomputer with associated system and program disk drives, tape reader, and terminal. Conventional disk management and program overlay techniques make it possible to handle an extensive data base. The hard copy output device (Versatec Incorporated "Matrix") may be operated as a conventional line printer or as a high resolution plotter. In the latter mode, images are built up and stored on disk until the analysis has been completed, then printed continuously.

Presentation of Data

There are a number of alternatives for displaying the spatial variation of sheet resistance data. These include one-dimensional profiles, two-dimensional maps (1, 4, 6, 8-10), and three-dimensional perspective drawings (3, 9, 10). Discussion in this section is restricted to the one- and two-dimensional formats, since these are considered by the authors to be more easily interpreted than perspective drawings, particularly for smoothly varying data.

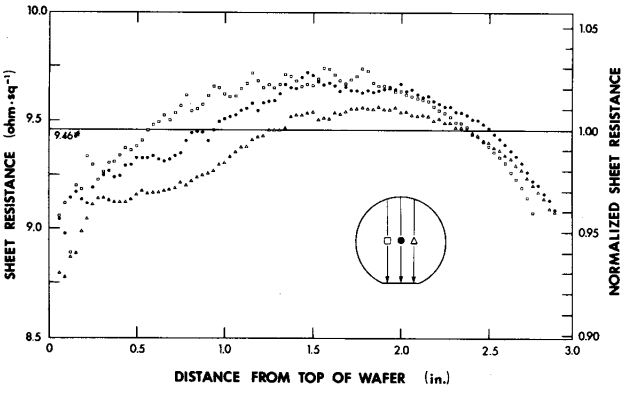

Fig. 2. One-dimensional FPP sheet resistance profiles for a phosphorus-diffused wafer ($\bar{\rho}_s$ = 9.46 Ω/sq and σ^*(%) = 2.47%).

One-dimensional profiles.—Figure 2 illustrates the variation in sheet resistance from top edge to bottom edge of a 3 in. diameter p-type silicon wafer doped with phosphorus from a phosphine diffusion source. Three parallel profiles (ΔX = 444 mil, ΔY = 30 mil) have been obtained using an in-line FPP (11) oriented perpendicular to the direction of travel. The solid line (9.46 Ω/sq) represents the mean sheet resistance as determined by averaging data from 118 sites on the wafer, as described below. The scale on the right side of the figure represents the fractional deviation from the wafer mean and permits comparison with the equivalue contour map discussed below.

One-dimensional profiles provide detailed information concerning the point-to-point variation in doping across the surface of a semiconductor wafer. They are particularly useful for exhibiting rapid local fluctuations such as are known to occur in ion-implanted wafers (1).

Two-dimensional maps.—The method of mapping sheet resistance variations employed by the authors involves measurements at 118 standard test sites located on the square grid shown in Fig. 3a. The distance between grid points is L = 222 mil for a 3 in. diameter wafer. The mean sheet resistance $\bar{\rho}_s$ and standard deviation σ are given by the expressions

$$\bar{\rho}_s = \frac{1}{118} \sum_{i=1}^{118} (\rho_s)_i \qquad [1]$$

and

$$\sigma^2 = \frac{1}{117} \sum_{i=1}^{118} [(\rho_s)_i - \bar{\rho}_s]^2 \qquad [2]$$

For an ideal gaussian distribution, ~95% of the data fall within two standard deviations of the mean. For this reason, the authors employ as a quantitative measure of the doping uniformity $\pm 2\sigma^* \times 100\%$, where the relative standard deviation σ^* is defined by the relation

$$\sigma^* = \frac{\sigma}{\bar{\rho}_s} \qquad [3]$$

After evaluating $\bar{\rho}_s$ and σ, the 118 sheet resistance values are displayed in one of the three formats which will now be described.

Deviation maps.—Figure 3b is an example of a deviation map for the same wafer for which one-dimensional profiles are plotted in Fig. 2. Deviations from $\bar{\rho}_s$ are computed according to the formula

$$\Delta_i(\%) = [(\rho_s)_i/\bar{\rho}_s - 1] \times 100\% \qquad [4]$$

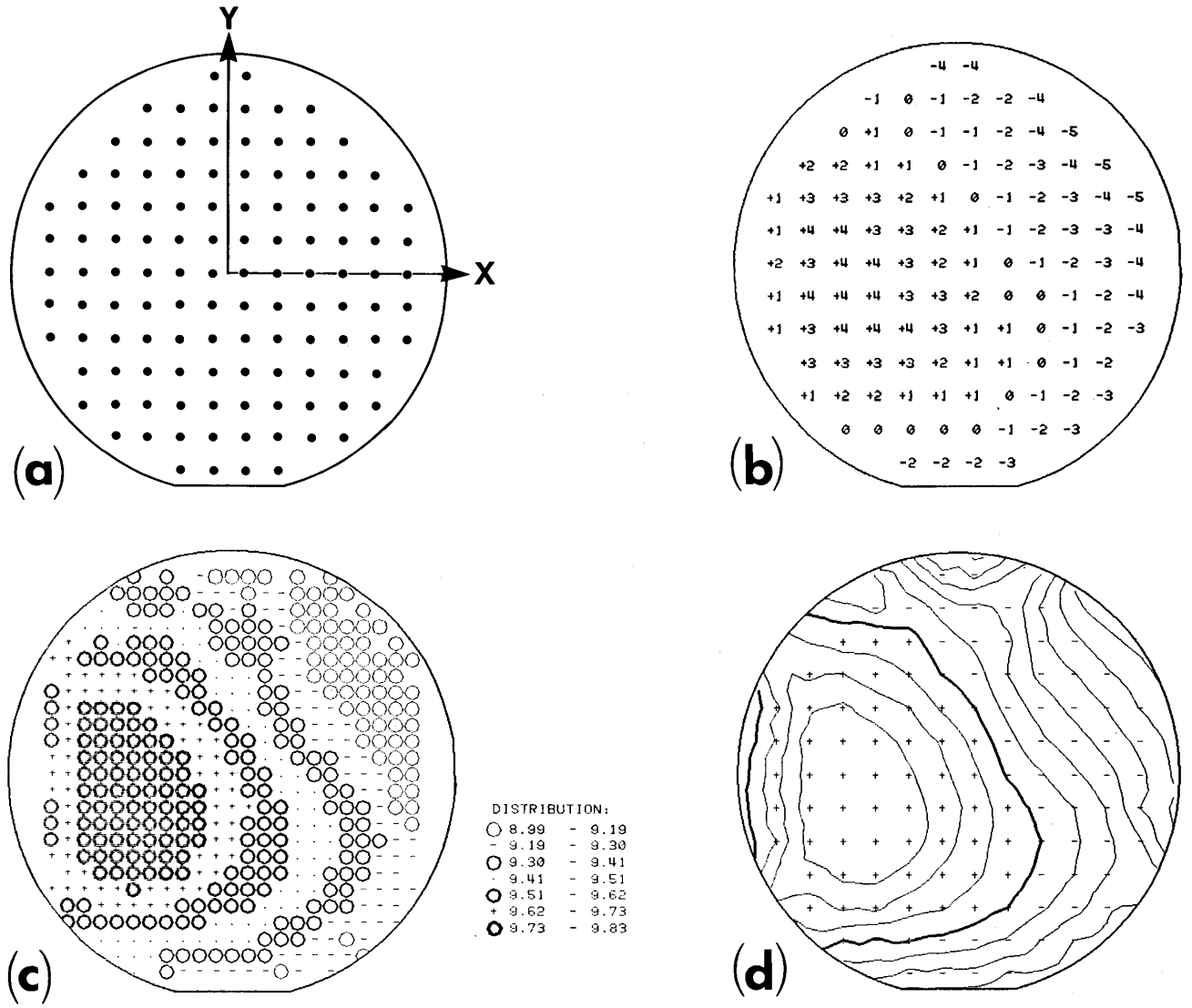

Fig. 3. Methods of displaying spatial sheet resistance variations: (a) standard 118 test site configuration; (b) percent deviation map; (c) histograph; (d) equivalue contour map. The data were obtained from FPP measurements of the wafer of Fig. 2.

rounded to the nearest integer value and plotted at the appropriate test site locations.

This display format requires the least amount of computation and can be implemented with a standard line printer. The underlying pattern of variation (Fig. 3c and 3d) may be observed by drawing smooth contour lines which enclose equal values of $\Delta_i(\%)$. (These contours may be drawn automatically using the graphic display techniques described in this paper.)

Histographs.—It is common practice to employ histograms to summarize the distribution of data over a range of values. Figure 3c is a histograph (two-dimensional histogram) which associates each measured value, and the interpolated values discussed below, with one of seven intervals into which the full range of experimental data has been divided. These intervals, each of which contains an equal number of values, are identified by circles of various line thicknesses and the symbols +, ·, and −. Unlike the deviation map, for which the +(−) sign identifies values which are above (below) the wafer mean, this method of display identifies values which are above (below) the wafer median.

The histograph succeeds in revealing the underlying pattern of variation by separating the data into seven bands of alternating character density.[2] In order to obtain continuous bands, it was necessary to first subdivide the initial network (Fig. 3a) by employing an interpolation scheme (described below) which results in a fourfold increase in the density of grid points. The distance between subgrid points for a 3 in. diameter wafer is 111 mil.

Equivalue contour maps.—Figure 3d shows an equivalue 1%-contour map obtained from the same data used for Fig. 3b and 3c. The heavy contour represents the mean sheet resistance $\overline{\rho_s}$, computed using Eq. [1], while the lighter contours differ from $\overline{\rho_s}$ in increments of 0.01 $\overline{\rho_s}$. The symbols +(−) identify experimental values which are greater (less) than $\overline{\rho_s}$. A curve representing the variation of ρ_s along any particular direction (as in Fig. 2) may be constructed by determining the points of intersection with the equivalue contours.

As in the case of the histographs discussed above, interpolation has been used to increase the density of grid points. This procedure assures that the contours, which are constructed from discrete line segments, will appear smoothly varying to the eye. In addition, a linear extrapolation scheme is utilized which allows contours to extend to the edge of the map.[3] These refinements help, in the opinion of the authors, to make

[2] A similar approach is employed in Ref. (10), in which the magnitude of a parameter is indicated by the darkness of the position characters.

[3] The contours drawn near the edge of the map may not be quantitatively correct since resistance values may change more rapidly near the edge of the wafer than over its interior. The extrapolation procedure is justified, however, as an aid to achieving a qualitative appreciation of the spatial variation of the parameter.

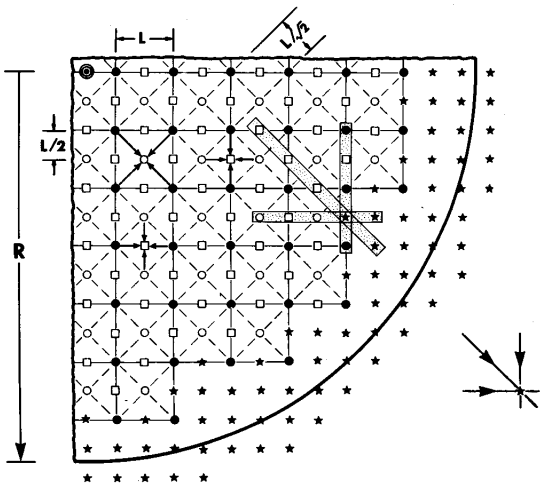

Fig. 4. Interpolation and extrapolation of data in the lower right quadrant of the wafer. The principal directions along which extrapolation is carried out are shown at the lower right.

equivalue contour maps the most effective means of displaying the patterns of spatial variation which are characteristic of semiconductor doping processes.

Interpolation and extrapolation of data.—Figure 4 illustrates the manner in which interpolation is carried out in the lower right quadrant of the wafer. A subgrid with cell parameter $L/2$ is obtained from the initial network of data points (●) in two stages. The first stage involves averaging the four experimental data points at the corners of the original grid cell to obtain the values represented by the symbol ○. This procedure results in a new grid rotated through 45° and having a cell parameter $L/\sqrt{2}$. The second stage involves averaging the four values at the corners of each $L/\sqrt{2}$ grid cell to obtain new values identified by the symbol □.

At the periphery of the expanded data array, extrapolation is used to obtain those subgrid values (★) which cannot be generated by the four-corner averaging technique described above. One estimate at an empty subgrid site is obtained by employing a least squares linear fit to a set of four nearby data points lying along one of the principal directions shown in Fig. 4. Using estimates obtained for the other two principal directions, one computes an average value for the sheet resistance at that point on the wafer. An example of this treatment of the data is shown in Fig. 4 for the case of the empty site nearest the center of the wafer. (In this instance, only three values are used along two of the principal directions, since the fourth value corresponds to an empty site.) This procedure is carried out, one site at a time, always filling the empty site nearest to the center of the wafer. Off-wafer sites are also filled in order to allow equivalue contours to extend to the wafer boundary, thereby significantly improving the comprehensibility of the contour map.

Measurement error.—The influence of random measurement error on the one-dimensional profiles in Fig. 2 is revealed by the scattering of data points. In a two-dimensional equivalue contour map, random error is manifested by irregular, distorted, or—in extreme cases—isolated contours. A technique for experimentally determining random error and the effect of such error on equivalue contour maps will now be discussed.

Experimental assessment.—The most direct way to assess random error is to determine the variation among a series of independent measurements of the sheet resistance. The procedure employed by the authors is illustrated in Table I, which summarizes a series of independent FPP (11) sheet resistance measurements made at nine different locations in a 3 × 3 square array ($\Delta X = \Delta Y = 120$ mil) centered on the phosphorus-diffused wafer for which data are presented in Fig. 2 and 3. After recording the first ($j = 1$) set of nine readings (probes along the X axis), the FPP is returned to its initial position, displaced 2 mils along the X axis, and a second ($j = 2$) set of nine readings recorded. This procedure is repeated until five readings have been obtained at each location. Each set of five readings is in turn used to compute a local standard deviation given by the expression

$$(\sigma_e)_i^2 = \frac{1}{4}\sum_{j=1}^{5}[(\rho_s)_{ij} - (\bar{\rho_s})_i]^2 \qquad [5]$$

where $(\bar{\rho_s})_i$, the local mean sheet resistance, is

$$(\bar{\rho_s})_i = \frac{1}{5}\sum_{j=1}^{5}(\rho_s)_{ij} \qquad [6]$$

These nine standard deviations are then used to compute an average standard deviation of the measurement error according to the formula

$$\sigma_e^2 = \frac{1}{9}\sum_{i=1}^{9}(\sigma_e)_i^2 \qquad [7]$$

When comparing values of σ_e for wafers of different sheet resistance, it is convenient to employ the relative standard deviation of the measurement error

$$\sigma_e^* = \frac{\sigma_e}{(\bar{\rho_s})_e} \qquad [8]$$

where $(\bar{\rho_s})_e$ is the average sheet resistance for the 45 measurements. The value $\sigma_e^*(\%) = 0.136\%$ obtained from Table I is typical of the random measurement error which the authors experience with a 25 mil FPP assembly on layers having sheet resistance ≤ 500 Ω/sq.

Effect on contour maps.—The effect of measurement error on a two-dimensional display format may be simulated by systematically introducing randomness into a set of data, $P(X, Y)$, whose relative standard deviation is $\sigma_P^* = \sigma_P/\overline{P}$. The influence of measurement

Table I. An example of the determination of FPP measurement error for the phosphorus-diffused wafer of Fig. 2 and 3. According to Eq. [7], $\sigma_e^*(\%) = 0.136\%$.

Probe location† X (mils)	Y (mils)	i	$(\bar{\rho_s})_i$ (Ω/sq)	$(\sigma_e^*)_i$, (%)	$(\rho_s)_{i1}$ (Ω/sq)	$(\rho_s)_{i2}$ (Ω/sq)	$(\rho_s)_{i3}$ (Ω/sq)	$(\rho_s)_{i4}$ (Ω/sq)	$(\rho_s)_{i5}$ (Ω/sq)
−120	120	1	9.696	0.131	9.717	9.690	9.700	9.686	9.690
0	120	2	9.681	0.187	9.691	9.653	9.680	9.679	9.701
120	120	3	9.647	0.103	9.657	9.634	9.653	9.652	9.639
−120	0	4	9.707	0.095	9.691	9.711	9.706	9.714	9.711
0	0	5	9.698	0.168	9.685	9.693	9.685	9.702	9.724
120	0	6	9.675	0.100	9.663	9.686	9.667	9.677	9.680
−120	−120	7	9.719	0.123	9.709	9.724	9.705	9.733	9.725
0	−120	8	9.720	0.189	9.700	9.709	9.718	9.725	9.748
120	−120	9	9.703	0.071	9.699	9.714	9.700	9.705	9.696

† The location $X = 0$, $Y = 0$ represents the center of the wafer.

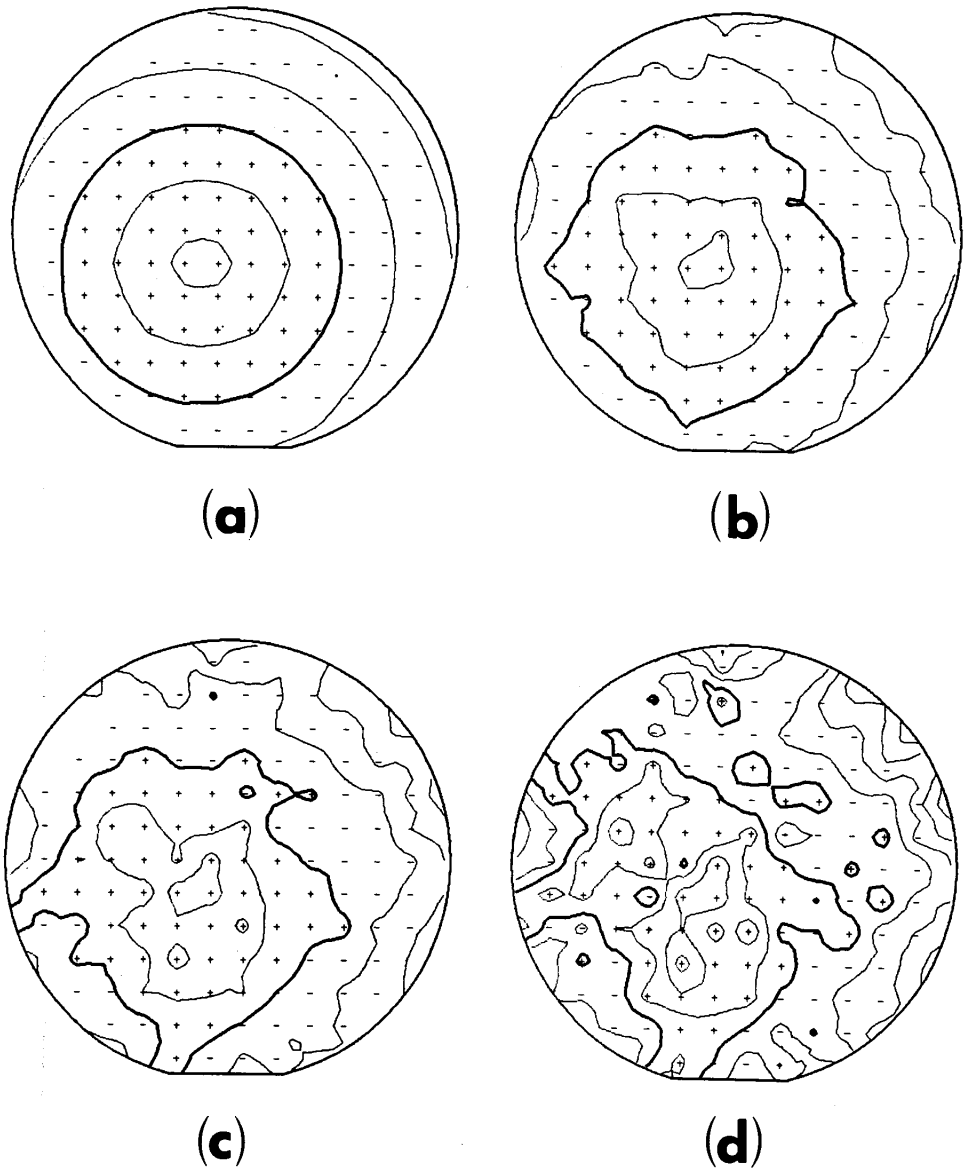

Fig. 5. The effect of random error of magnitude $\sigma_\epsilon^*(\%)$ on a hypothetical distribution for which the over-all uniformity is $\sigma_P^*(\%) = 1.00\%$: (a) $\sigma_\epsilon^*(\%) = 0$; (b) $\sigma_\epsilon^*(\%) = 0.25\%$; (c) $\sigma_\epsilon^*(\%) = 0.50\%$; (d) $\sigma_\epsilon^*(\%) = 1.00\%$.

error is simulated by adding to each of the 118 $P(X, Y)$ values a random number $\epsilon(X, Y)$ selected from a normal distribution with a nominal mean of 0 and a relative standard deviation $\sigma_\epsilon^* = \sigma_\epsilon/\bar{P}$.

Examples of this procedure for various values of σ_ϵ^* are shown in Fig. 5a-5d for the case of a pattern of concentric circles (note similarity to Fig. 3d) for which $\sigma_P^*(\%) = 1.00\%$. As σ_ϵ^* increases in magnitude, the contours become progressively less regular until a point is reached at which it is no longer possible to recognize the underlying pattern of variation shown in Fig. 5a. This point appears to occur when $\sigma_\epsilon^*(\%) \approx 0.50\%$, since the underlying pattern, which can be detected in Fig. 5b despite the irregular contours, can no longer be identified in Fig. 5c. Figure 5d illustrates the consequences of the measurement error becoming comparable to the intrinsic variability of the data. Not only have the circular contours become so distorted that they reach the edge of the wafer map, but many isolated regions have appeared as a result of large excursions from the correct local behavior.

Measurement Techniques

In this section the FPP and van der Pauw resistors are discussed from the perspective of producing data suitable for mapping sheet resistance variations. A special test mask is then described which incorporates both vehicles on the same wafer, making it possible to carry out a direct experimental comparison.

FPP measurements.—It is common practice to employ an in-line FPP, as shown in Fig. 6, for characterizing the sheet resistance of doped semiconductor wafers (5, 6). If the probe separation distance s is at least twice the thickness of the layer being measured, then

$$\rho_s = k\frac{\Delta V}{I} = kR \qquad [9]$$

where k is a geometrical correction factor which depends on the location of the probes and the shape of the sample, I is a current through two of the probes, ΔV is the potential difference measured between the remaining two probes, and the resistance R is defined

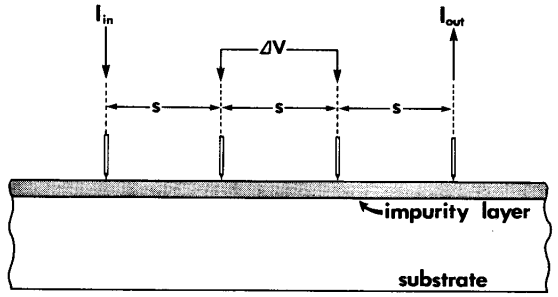

Fig. 6. Conventional current/voltage configuration for an in-line FPP array.

as $\Delta V/I$ (12). Ordinarily, the outer two electrodes of the in-line FPP carry current and the inner two electrodes are used to measure voltage since, for an FPP having equal distances of separation between the probe needles, this assignment results in the largest value of ΔV (13).

Logan (14) has shown that a circular sample doped on both sides (such as the phosphorus-diffused wafer described above) should behave as if its front surface were part of a continuous infinite sheet. Thus the correction factor is a constant value ($k = \pi/\ln 2 = 4.532$), independent of the location of the FPP. In contrast, a thin circular sample doped on one side will require knowledge of the orientation and position of the probe array in order to utilize Eq. [9]. General expressions have been derived for the case of the FPP oriented along the radius (14) and for the FPP oriented perpendicular to the radius (15) of a thin circular sample. Perloff (6) has derived expressions for the FPP oriented at an arbitrary angle with respect to the wafer radius, making it possible to employ automatic wafer probing equipment for evaluating doping uniformity.

An alternative approach to FPP measurements, which is particularly useful for ion-implanted wafers, involves the application of photolithographic techniques to define rectangular regions of sufficient size to accommodate the FPP array, as shown in the cross-sectional view of Fig. 7a. If an automatic wafer probing apparatus is employed to position the FPP so that it occupies the same relative location in each pattern (Fig. 7b), k will assume a constant value over the entire wafer. When the FPP is positioned equidistant from the edges of a rectangular test pattern (RTP), the solution furnished by Smits (12) may be employed to compute the correction factor. Figure 8 is a plot of k *vs.* $b/3s$ for the case of an in-line FPP, probe separation s, situated symmetrically within RTP's of length b and width a. The magnitude of k, for fixed values of the ratio $b/3s$, decreases rapidly as the aspect ratio b/a increases. Experimental points were obtained for

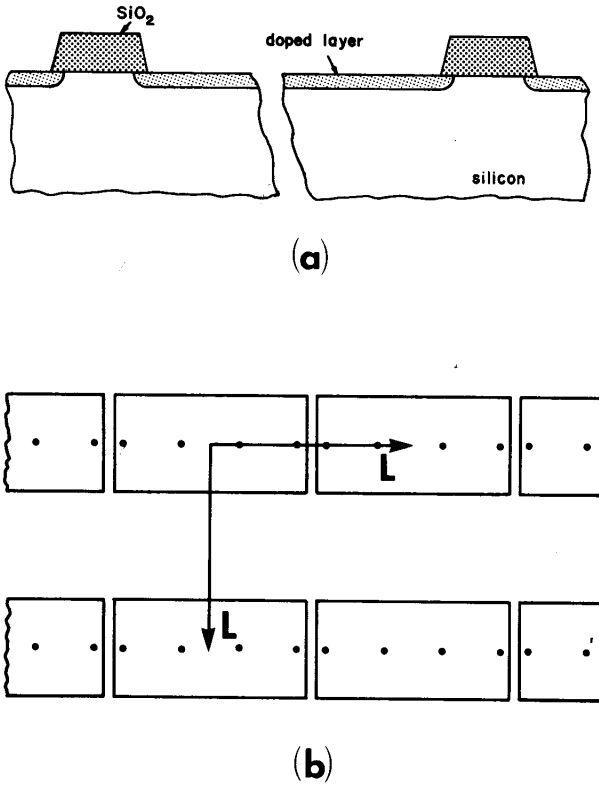

Fig. 7. Rectangular test patterns used in conjunction with an in-line FPP to eliminate variations in correction factor: (a) cross section through test pattern; (b) arrangement of patterns on a square grid (L = 222 mil for a 3 in. diameter wafer).

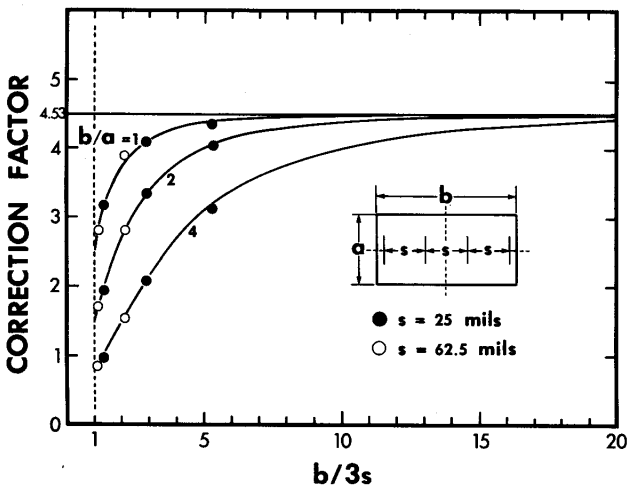

Fig. 8. Correction factor k *vs.* $b/3s$ for a FPP symmetrically positioned within a rectangular test pattern of length b and width a.

various size RTP's using FPP assemblies for which s = 25 and 62.5 mil.

The sensitivity of the FPP to small doping variations is illustrated in Fig. 9a which represents a typical pattern of variability obtained for a 3 in. diameter n-type silicon wafer implanted with boron in a mechanically scanning implantation system (1). (These data were obtained by employing an s = 62.5 mil FPP in conjunction with 220 × 110 mil² RTP's.) Figure 9b represents the pattern predicted on the basis of small changes in the linear velocity of the wafer as it traverses a stationary ion beam. This pattern, which is unique to the Ferris wheel mechanism employed for moving the wafers, corresponds extremely well to the experimental results of Fig. 9a. The irregularity in the contours of Fig. 9a is, as discussed above, a consequence of random error in the experimental sheet resistance data. The effect is not, however, significant enough to impair the interpretation of the resulting contour map.

The use of the FPP for evaluating the sheet resistance of junction isolated implanted layers has been discussed by Stephen (16) who identified the following sources of error when making such measurements: surface effects, junction leakage, geometrical factors, magnitude of the measuring current, probe loading, and ambient temperature. In practice, by employing commercially available "precision" probe assemblies and restricting the measurement to layers greater than 2000Å in thickness and less than 500 Ω/sq, one can achieve an absolute accuracy of ±1% and a $\sigma_e^*(\%) \leqq 0.5\%$. The primary source of error, under these circumstances, is associated with variation in the distances between adjacent probe needles due to mechanical tolerances of the probe assembly (17).

Van der Pauw resistor measurements.—The FPP cannot conveniently be used to evaluate a series of doping steps on the same test wafer, as would be desirable when examining the spatial variation of device parameters. Van der Pauw (7) has described a resistor geometry which can be fabricated simultaneously with active devices and should be insensitive to variations in both the photomask and the exposure and etching steps used to delineate the pattern. The sheet resistance of a van der Pauw resistor is determined from the relation

$$\rho_s = \frac{\pi}{\ln 2}\,\frac{R_a + R_c}{2}\,f(R_a/R_c) \qquad [10]$$

where, with reference to Fig. 10, $R_a = \Delta V_{23}/I_{14}$, $R_c = \Delta V_{43}/I_{12}$, and the function $f(R_a/R_c)$ satisfies the transcendental expression

$$\frac{R_a/R_c - 1}{R_a/R_c + 1} = \frac{\cosh^{-1}[(1/2)\exp(\ln 2/f)]}{\ln 2/f} \qquad [11]$$

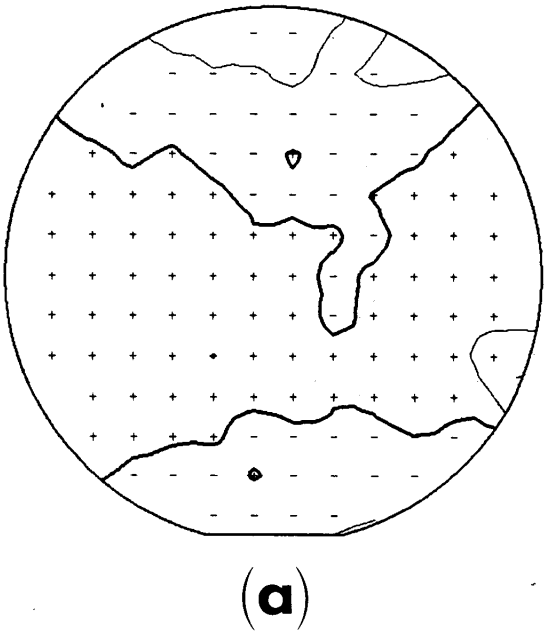

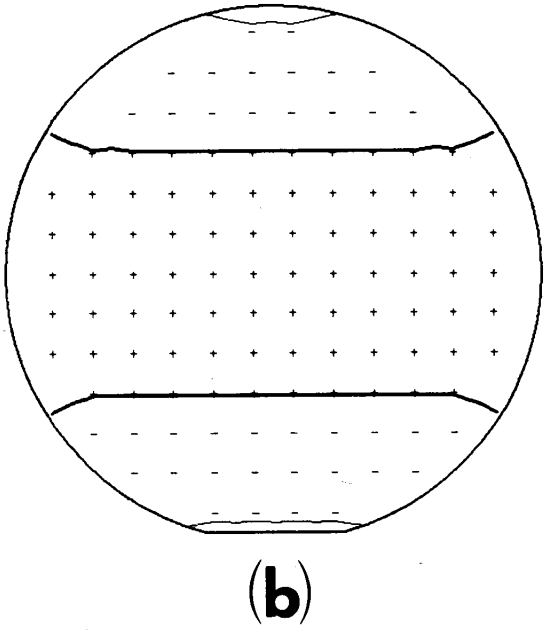

Fig. 9. Pattern of variation for a wafer implanted in a mechanically scanning system: (a) experimental results ($\sigma^*(\%) = 0.50\%$, $\bar{\rho}_s = 34.5$ Ω/sq; (b) predicted behavior ($\sigma^*(\%) = 0.35\%$).

A third current/voltage configuration, $R_b = \Delta V_{24}/I_{13} = R_a - R_c$, is ordinarily used for Hall effect measurements. For a symmetric pattern and symmetrically arranged contacts, one has that $R_a = R_c$ and consequently $f(R_a/R_c) = 1$.

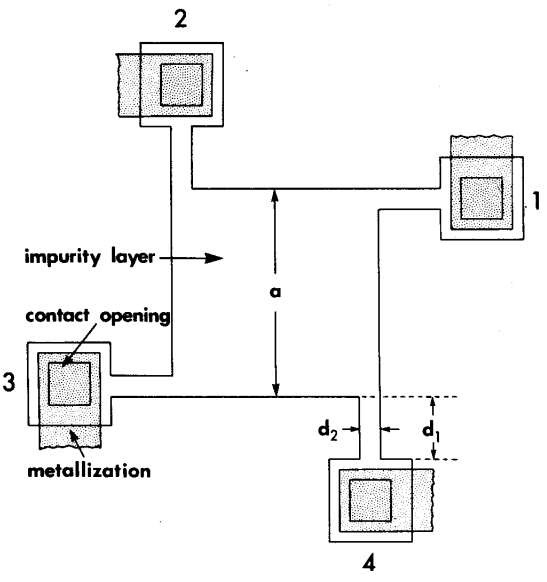

Fig. 10. Van der Pauw four-point resistor structure

Van der Pauw's analysis is based on the assumption of point contacts. In practice, however, one is obliged to make contact to the body of a van der Pauw resistor through arms of finite width. David (18) has determined the error associated with measuring the sheet resistance of a structure with orthogonal boundaries and finite-width contact arms. For the offset quadrate cross shown in Fig. 10, which is the geometry employed in the National Bureau of Standards process evaluation mask set (NBS-3) (19), Eq. [10] is correct to better than 0.1% as long as the requirement $d_1/a \geq d_2/a$ is fulfilled.

Comparison of FPP and van der Pauw measurements. —In order to compare directly FPP and van der Pauw measurements, the authors have employed a specialized test mask which permits both types of measurements to be made at each of the 118 standard test sites shown in Fig. 3a. A 212 × 50 mil² RTP, designed to accommodate a 62.5 mil FPP, and four different size van der Pauw resistors of the design shown in Fig. 10 are employed for this comparison. For each size van der Pauw resistor, three identical structures are clustered as close together as possible to facilitate a determination of random measurement error.

Table II summarizes the results of an evaluation of a 3 in. diameter boron-implanted (150 keV, 5×10^{14} cm^{-2}) n-type silicon wafer. The excellent agreement among values of ρ_s and $\sigma^*(\%)$, for structures varying in area over almost five orders of magnitude, is typical of the comparative behavior observed by the authors at impurity concentrations above ~10^{18} cm^{-3}. Figure 11 compares equivalue contour maps constructed from data for (a) the 10 × 10 μm² van der Pauw resistor, (b) the 100 × 100 μm² van der Pauw resistor, and (c) the 5400 × 1260 μm² = 212 × 50 mil² RTP. These maps, which convey essentially identical information about

Table II. Comparison of FPP and van der Pauw resistor† data for a boron-implanted n-type silicon wafer

Test pattern	a (μm)	b (μm)	$A = a \times b$ $(\mu m)^2$	$\bar{\rho}_s$ (Ω/sq)	$\sigma^*(\%)$	$\sigma_e^*(\%)$ 1-config.	$\sigma_e^*(\%)$ 2-config.
vdP-1	10	10	1.0×10^2	168.91	1.55	0.832§	0.020§
vdP-2	35	35	1.2×10^3	167.99	1.48	0.292	0.046
vdP-3	100	100	1.0×10^4	168 95	1.47	0.267	0.021
vdP-4	500	500	2.5×10^5	168.70	1.45	0.078	0.057
RTP‡	1260	5400	6.8×10^6	167.62	1.56	0.057	—

† The van der Pauw geometry is shown in Fig 10. The arm length $d_1 = 30$ μm and the arm width $d_2 = 10$ μm for each of the four patterns.
‡ Data obtained using a 62.5-mil FPP.
§ Cf. Table III.

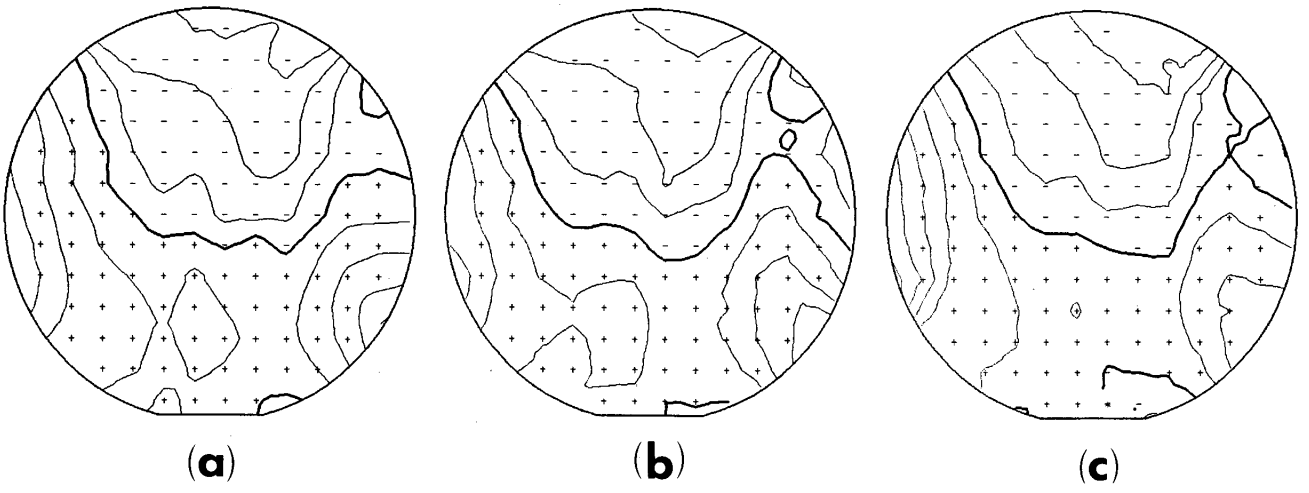

Fig. 11. Two-configuration equivalue contour maps for the boron-implanted wafer of Table II: (a) 10 × 10 μm^2 van der Pauw resistor; (b) 100 × 100 μm^2 van der Pauw resistor; (c) 5400 × 1260 μm^2 rectangular FPP test pattern.

the spatial variation of sheet resistance, demonstrate conclusively that the FPP and van der Pauw resistors may be used interchangeably. [Changes in the velocity of the wafer in a mechanically scanning implantation system employing track-mounted wafer carriers are responsible for the distinctive pattern (1).]

As discussed in the preceding section, random error plays an important role in determining the visual quality of equivalue contour maps. Table II provides results for $\sigma_e^*(\%)$ for the five different test structures. The van der Pauw resistor data were obtained by measuring the three "identical" structures for each of the four resistor sizes at nine different wafer locations. The FPP data were obtained by performing five independent measurements on each of nine different RTP's.[4] It is clear that the use of two independent current/voltage configurations leads to a dramatic reduction in $\sigma_e^*(\%)$ for each size van der Pauw resistor but particularly for the 10 × 10 μm^2 resistor, for which the one-configuration value is 0.832% and the two-configuration value is 0.020%. It is noteworthy that even the 500 × 500 μm^2 van der Pauw resistor is influenced by geometric variations to a small extent as evidenced by the one-configuration value of 0.078% *vs.* the two-configuration value of 0.057%. The value of 0.057% for the FPP measurements compares favorably with the two-configuration values for the van der Pauw resistors.

The importance of using two-configuration data for small van der Pauw resistors may be appreciated by comparing the maps of Fig. 12, representing $4.532R_a$ and $4.532R_c$ data for the 10 × 10 μm^2 resistor, with the map of Fig. 11a, which was constructed by combining these data in accordance with Eq. [10]. The contour maps of Fig. 12 exhibit the influence of random error as irregular contours and isolated features, just as occurs in the measurement error simulations of Fig. 5c and 5d.

Table III summarizes the measurement error data used to compute $\sigma_e^*(\%)$ for the 10 × 10 μm^2 van der Pauw resistor. The large variation among the one-configuration values $(\rho_s)_{i1}$, $(\rho_s)_{i2}$, and $(\rho_s)_{i3}$ is attributed to fluctuations in photolithography and etching which cause the dimensions of nominally identical structures to vary randomly. The variability which still remains in the two-configuration data is associated, at least for the 10 × 10 μm^2 resistor, with the finite resolution of the digital voltmeter and stability of the current supply. This conclusion is based on the fact that, irrespective of resistor size, repeated measurements of the same van der Pauw resistor lead to values of $\sigma_e^*(\%)$ in the range 0.015-0.020% for both the one- and two-configuration cases. Additional sources of variability are attributed to local gradients in sheet resistance, junction leakage current, and changes in ambient temperature. Some of these effects may be influencing σ_e^* for the larger van der Pauw resistors, particularly local resistivity gradients, since these would be expected to become more important as the center-to-center spacing between patterns increases.

Conclusion

The results of this investigation demonstrate that both the conventional FPP and van der Pauw resistors of microelectronic dimensions are suitable for use with automated wafer probing equipment for characterizing the doping uniformity of semiconductor wafers. Both vehicles are capable of providing sheet resistance data sufficiently free of random measurement error to

[4] The FPP was displaced in 2 mil increments parallel to the 212 mil side of the RTP, with the third repetition corresponding to the symmetry position. The geometric error inherent in this choice of probe locations is not a significant contribution to the measured value of σ_e^*.

Table III. An example of the determination of measurement error for resistor vdP-1 of Table II. According to Eq. [7], $\sigma_e^*(\%) = 0.832\%$ for the one-configuration case and 0.020% for the two-configuration case.

Probe location†			1-configuration					2-configuration				
X (mils)	Y (mils)	i	$(\overline{\rho_s})_1$ (Ω/sq)	$(\sigma_e^*)_1$ (%)	$(\rho_s)_{i1}$ (Ω/sq)	$(\rho_s)_{i2}$ (Ω/sq)	$(\rho_s)_{i3}$ (Ω/sq)	$(\overline{\rho_s})_1$ (Ω/sq)	$(\sigma_e^*)_1$ (%)	$(\rho_s)_{i1}$ (Ω/sq)	$(\rho_s)_{i2}$ (Ω/sq)	$(\rho_s)_{i3}$ (Ω/sq)
−222	222	1	172.15	0.763	170.94	173.55	171.96	171.93	0.022	171.96	171.90	171.95
0	222	2	172.82	0.619	173.32	173.55	171.59	171.09	0.019	171.11	171.08	171.08
222	222	3	170.09	1.069	168.45	172.05	169.78	170.01	0.027	170.00	169.97	170.05
−222	0	4	172.51	0.453	173.18	171.65	172.70	171.81	0.015	171.84	171.79	171.80
0	0	5	170.88	0.540	171.90	170.60	170.12	171.46	0.000	171.45	171.46	171.46
222	0	6	170.87	0.901	170.66	172.50	169.44	170.72	0.014	170.71	170.71	170.74
−222	−222	7	169.83	1.272	170.18	171.79	167.51	171.19	0.032	170.24	171.12	171.20
0	−222	8	170.50	0.653	170.88	169.24	171.37	171.03	0.000	171.03	171.01	171.05
222	−222	9	169.87	0.898	171.00	170.49	168.14	170.69	0.022	170.71	170.64	170.70

† The location $X = 0$, $Y = 0$ represents the center of the wafer.

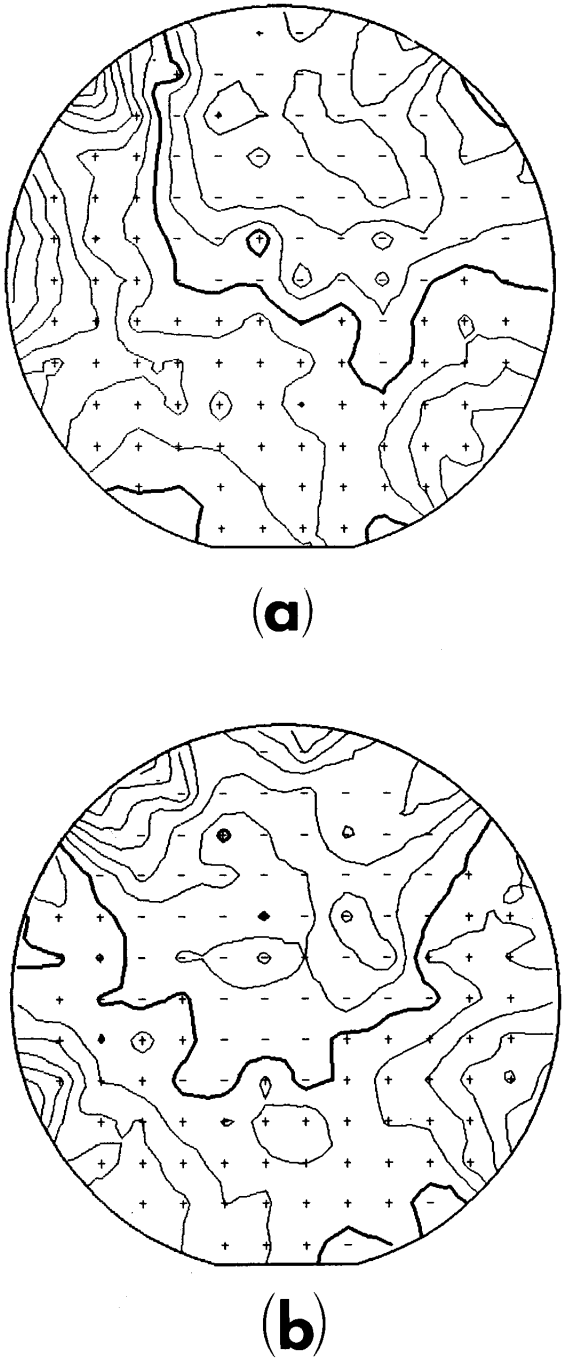

Fig. 12. One-configuration equivalue contour maps for the 10 × 10 μm^2 van der Pauw resistor corresponding to the two-configuration map of Fig. 11a.

justify the use of high resolution two-dimensional graphic display techniques.

The procedure employed for assessing the random error associated with four-point resistance measurements may be applied to any device or process parameter for which it is possible to carry out a series of independent measurements at various locations on the semiconductor wafer. By evaluating the relative measurement error in this way, one may predict the extent to which graphic display techniques will be an effective means of exhibiting spatial variations.

Acknowledgments

The authors wish to acnowledge the able assistance of Mr. D. Mar in the areas of mask design and wafer characterization. Technical discussions with Mr. J. D. Reimer, Dr. J. T. Kerr, Dr. J. A. Marley, Dr. S. W. Mylroie, Dr. H. J. Sigg, and Dr. M. G. Buehler (National Bureau of Standards) have been extremely valuable both in carrying out this investigation and preparing the results for presentation.

Manuscript submitted Oct. 4, 1976; revised manuscript received Nov. 6, 1976.

Any discussion of this paper will appear in a Discussion Section to be published in the December 1977 JOURNAL. All discussions for the December 1977 Discussion Section should be submitted by Aug. 1, 1977.

Publication costs of this article were assisted by Signetics Corporation.

REFERENCES

1. D. S. Perloff, F. E. Wahl, and J. T. Kerr, in Proceedings of 7th International Conference on Electron and Ion Beam Science and Technology, Washington, D.C., 1976.
2. G. Kelson, H. H. Stellrecht, and D. S. Perloff, *IEEE J. Solid-State Circuits*, **sc-8**, 396 (1973).
3. P. A. Crossley and W. E. Ham, *J. Electron. Mater.*, **2**, 465 (1973).
4. D. S. Perloff, F. E. Wahl, and J. D. Reimer, *Solid State Technol.*, **20**, 31 (Feb. 1977).
5. L. B. Valdes, *Proc. Inst. Radio Engrs.*, **42**, 420 (1954).
6. D. S. Perloff, *This Journal*, **123**, 1745 (1976).
7. L. J. van der Pauw, *Philips Res. Rep.*, **13**, 1 (1958).
8. M. G. Buehler and W. R. Thurber, *IEEE Trans. Electron Devices*, **ed-23**, 968 (1976).
9. G. Wolfe, *Circuits Manufacturing*, **16**, 48 (April 1976).
10. W. E. Ham, *Nat. Bur. Stand. Spec. Publ. 400-15*, pp. 25-34 (January 1976).
11. Manufactured by A. M. Fell Ltd., London, England.
12. F. M. Smits, *Bell Syst. Tech. J.*, **37**, 711 (1958).
13. R. Rymaszewski, *J. Sci. Instrum.*, **2**, 170 (1969).
14. M. A. Logan, *Bell Syst. Tech. J.*, **40**, 885 (1961).
15. L. M. Swartzendruber, *Solid-State Electron.*, **7**, 413 (1964).
16. G. Dearnaley, J. H. Freeman, R. S. Nelson, and J. Stephen, "Ion Implantation," North Holland, Amsterdam (1973).
17. F. E. Wahl and D. S. Perloff, Unpublished results.
18. J. M. David, *Nat. Bur. Stand. Spec. Publ. 400-19*, p. 44 (April 1976).
19. M. G. Buehler, *Nat. Bur. Stand. Spec. Publ. 400-15*, pp. 35-46 (January 1976).